X-ray Mapping and Interpretation of Scatter Diagrams

Ken Moran [1,2] and Richard Wuhrer [2]

[1] Moran Scientific Pty Ltd, 4850 Oallen Ford Road, Bungonia, NSW, 2580, Australia.

E-mail: kmoran@goulburn.net.au

[2] Microstructural Analysis Unit, University of Technology, Sydney, P.O. Box 123,

Broadway, NSW 2007, Australia. E-mail: Richard.Wuhrer@uts.edu.au

1. Abstract

Quantitative x-ray mapping (XRM) has become a very useful characterisation tool for determining the elemental distribution in materials, whether using energy dispersive spectroscopy (EDS) or wavelength dispersive spectroscopy (WDS). The intensity distributions of the elements from an x-ray map allow us to generate two dimensional and ternary scatter diagrams thus converting spatial information into concentration dimensions, which is an important tool for displaying the spatial relationships of elements or correlated elements (phases) in materials. To best understand how to use this tool, we need to understand the production and features of the scatter diagram. The type of clustering observed in the scatter diagram, whether oval, linear or spherical, can give the major and trace element distributions within phases as well as qualitative and quantitative phase information. This paper demonstrates the generation of scatter diagrams, properties of scatter diagrams, interpretation of scatter diagrams and the advantages of scatter diagrams through the use of examples.

Keywords

Correlation diagram, scatter diagrams, x-ray mapping, intensity histograms

2. Introduction

X-Ray Mapping (XRM) and more importantly quantitative x-ray mapping (QXRM) are powerful characterization techniques aiding in the understanding of the spatial distribution of elements in materials. However, much of the quantitative information is extremely complex and as such is enormously difficult to reproduce as a single image. What is required is a method that can select quantitative concentration data and be able to show where this concentration data exists on a spatial distribution. A simple intuitive method to accomplish this is through the use of two and three-dimensional (2D and 3D) scatter (or correlation) diagrams, which are generated from the x-ray maps [1-3]. Simple two-dimensional scatter diagrams are where pixel frequency versus element concentration profiles are plotted against each other for selected elements within the sample. It is also possible to create two-dimensional ternary scatter diagrams as well as more complicated three-dimensional (3D) rotation diagrams and 3D data cubes.

From these scatter diagrams we observe clusters, also referred to as nodes, which correspond to different chemical phases. We can also observe linking (connection) between clusters indicating the boundaries between phases within a material as well as branching from clusters (some links may contain branches). Branching is defined as a link with a node at one end only, and is often referring to solid solutions (compositional variations) of the same phase or separate phases of similar solid solution. The contributing pixels to each cluster can be used

to reconstruct the spatial distribution of its associated chemical phase or boundary in a chemical image of the specimen. In other words, from the scatter diagram you can select a cluster of points and then display these points redrawn on the electron image. The new image shows the selected analysis points superimposed on the electron image, which was collected while mapping, giving perfect correlation. The scatter diagrams may be derived from region of interest mapping (ROIM) or quantitative XRM (QXRM).

Selecting areas on the scatter diagrams and observing where the points lie on the image is a very important part of the phase identification process. These selected analysis points may then be summed for a more accurate analysis in total or by selecting strategic areas on the image. Selecting areas on the electron or x-ray image and showing where these points plot (retrace) on the scatter diagrams is also important in locating missing clusters. It is best to use as many different methods as possible, such as pseudo colouring, ratio imaging and principal component analysis (PCA) to determine where the phases of interest are. Once other phases are located on the scatter (correlation) diagram, we can then determine where all similar concentration areas appear on the image. From the clusters observed in the scatter diagram, it is possible to map the phases. This is often referred to as phase mapping, but really it should be called chemical phase mapping (CPM), as phase mapping assumes knowledge of atomic positions and requires diffraction analysis. The XRM method that we are describing uses chemistry through use of either EDS and/or WDS analysis. It is also important to recognise that all elements need to be mapped, as some phases are determined from very minor elemental variation and even elements that are difficult to analyse. If a full spectrum at each pixel is saved, this makes the process of looking for other elements much easier.

The phases found through XRM can be further verified through use of other techniques, such as x-ray diffraction (XRD) and electron backscattered diffraction (EBSD). EBSD is one of the best techniques available for structural phase mapping, as it will discriminate on the basis of unit cell dimension and orientation. This is fine if you have the specimen that is able to be prepared correctly and has a crystalline structure. Indeed, one of the major drawbacks with EBSD mapping is the sample preparation required.

3. Instrumentation

Current research work involves a multi-detector EDS and WDS x-ray mapping system incorporated on a Jeol 733 microprobe and a Jeol 35CF with two EDS detectors. The Jeol 733 is currently operating with three EDS x-ray detectors and three WDS detectors simultaneously. The Jeol 35CF has two EDS detectors that operate simultaneously and is currently being fitted with a WDS detector.

4. Generation of Scatter Diagrams

The generation of scatter diagrams is best understood by considering the information given in the linear intensity distribution histogram from each individual element. From this information, a two-dimensional scatter diagram is produced, which is a plot of the frequency of occurrence of intensity values for one element against another for each pixel in the x-ray map. To show this using a real sample, a three element system is shown in Figure 1 (SE plus three x-ray images). The three element configuration was chosen to keep to a simple system. An intensity histogram is created from the x-ray image for each element present (Figure 2)

and each intensity histogram shows the frequency with which each value of the image intensity occurs against the full range of intensity values. The two dimensional scatter diagrams are given an extra dimension by thermally colouring the intensity of points on the diagrams. This dimension indicates the number of points in the image with this concentration (Figure 3). Figure 4 shows all the scatter diagrams for the sample in Figure 1.

As can be seen in Figure 2, the intensity histograms can also reveal other information about the element distribution within the sample. Each peak in the intensity histogram represents one or more different phases. Each peak also represents a particular concentration of that element. Many different phases may have the same concentration of a particular element. This is especially the case for the zero peak. That is, many phases may have none of the element indicated present in the phase. Phases may also be present even though there is no obvious peak present in the intensity histogram, because of there being only a small volumetric amount of this phase present in the image. All sections of the histogram belong to a phase in the image. The broadness of the peak represents a number of features, such as statistics, variations of concentration, overlapping phases and it can also represent drift. The height, or area of the peak, represents an area on the image. For a quantified distribution, the peak around the zero value represents the concentration at or around zero percent of the element and is of significant interest. The red area on the left hand side of the histograms (Figure 2a and c) are negative values, which are part of the gaussian peak representing the zero peak. The right side of the histogram represents the maximum concentration of the element in the image. The total area of the histogram represents the total number of pixels in the image. In the examples given, all the floating point information, representing up to five

orders of magnitude of concentration, are compressed to a 0-255 grey scale for convenience. This does not always have to be the case.

Scatter diagrams can be produced from either region of interest (ROI) intensity distributions or from quantitative intensity distributions. The difference between the two types is that the quantitative scatter diagrams have had the background removed, overlaps corrected and intensity data corrected. To understand their power requires that we understand the linear interpretation of each individual elemental distribution. This distribution is complicated substantially by overlap and background removal. The illustrations in this paper are quantitative distributions and as such are complicated at the zero concentration limit. The correlation of the points in the scatter diagram creates clusters, also referred to as nodes. If these clusters represent distinct separated positions on the correlation diagram, then these clusters represent distinct phases with differing elemental concentration. On the other hand, the scatter diagrams can also show correlation or anti-correlation. That is, correlation is where as element *"a"* increases and element *"b"* increases and anti correlation is where *"a"* increases and *"b"* decreases or vice versa. They may also be vertical (*"a"* increases *"b"* remains the same) or horizontal (*"a"* remains the same *"b"* increases). These last two are common where elements *"a"* or *"b"* are at or near zero concentration. In Figure 5, results from an investigation of a slag material revealed complete dendritic growth of the magnesium rich phase. In this example there is an overlap between the dendritic growths and the calcium rich matrix. The scatter diagrams demonstrate direct calcium and titanium correlation (Figure 5d) while titanium and magnesium show anti-correlation (Figure 5e). On the other hand, if there are no points on the plot then there are no points on the image with this composition of

"a" and *"b"* observed. The vertical and horizontal lines (crosshairs) inside the plot area indicate the zero value lines on the diagram. These lines only appear on the quantitative scatter diagrams and will only contain these zero lines if there are concentration areas that are statistically near zero concentration. ROI scatter diagrams have no negative points on the plot. If the average of a cluster falls below the zero line then we know that the overlap or background removal function is in error. If the full spectrum at each pixel has been saved, then this can be easily corrected.

5. Properties of scatter diagrams

There are a number of very important aspects of scatter diagrams, as well as many considerations having to be taken into account, for correct interpretation of scatter diagrams. Of particular interest are:

(i) Individual clusters (or nodes) in each scatter diagram, the type or shape of the clusters (spherical clustering, oval clustering and linear clusters) and zoning.

(ii) Branches and links between clusters in each scatter diagram and how these features correlate the chemical distribution of elements both in and around the phase region.

(iii) Minor element distributions and the effect of the statistics of clusters and averaging.

i. Clusters (Nodes) and Types

On the scatter diagrams, clusters represent large numbers of pixels in the image with similar concentrations. Each cluster may represent one, or more, variable sized regions in the image. The number of points in a cluster directly relates to the area occupied by this phase in the image. The number of clusters in the scatter diagram represents the number of different

phases in the image. Furthermore, there may be more clusters in a ROI diagram than in a quantitative diagram. This is because, for quantitative plots, all the phases and their clusters with zero concentration exist as a single cluster at the zero concentration point (Figure 6e).

The spread of the points in each cluster may represent true concentration variations, artefacts and also be a measure of the statistical distribution of the intensity data at each pixel in the image. The position of the cluster gives the relevant concentration of the two elements in the correlation. However, there is often information within an individual cluster. For example, zoning within a phase can be determined by plotting sections of the cluster, as shown in Figure 6a-c and Figure 7. Zoning is often obvious once it has been identified and is where an area is different, in some respect, to adjoining areas. Figure 7 shows the x-ray maps and scatter diagram created from a cast iron sample for the chromium and iron elements. By selecting the lower section of the cluster (Figure 7c) a zoning region can be highlighted (Figure 7d).

Other phases within a cluster may also be determined by correlating with other major or minor elements. These may or may not have been initially analysed. An important method to determine, if this is the case, is to select areas on the image with subtle differences and see where these points lie on the scatter diagram.

Another important property of the scatter diagram is the shape of the clusters, which can also give very important information about the sample. There can be many different cluster shapes observed in a scatter diagram, but basically the three more common and important types are

spherical clustering, oval clustering and linear clusters. These may merge into each other in this order with no distinct delineation between them. For example, a spherical cluster often becomes oval shaped when the statistics of the sample are improved.

The presence of *spherical clustering* usually means that the concentration range and statistical error for both elements is the same or similar. Figure 6e shows a scatter diagram for a sample, which has cobalt and manganese present with similar composition. This scatter diagram reveals a spherical cluster about the zero composition point. This spherical cluster exists as a single cluster even though we know that multiple phases exist within this cluster.

The occurrence of *oval and linear clustering* on the scatter diagrams means that there may be a narrow to broad range respectively of concentrations (solid solution), or a mixture of spherical, oval or linear clusters plus boundaries. Figure 6 is an example of a hard facing material with tungsten carbide particles bonded to a steel substrate. The scatter diagram reveals not only oval clustering (with the upper region selected) but also a mixture of linear clustering and branching. As can be seen in Figure 6b, the upper region of an oval cluster has been selected and the image formed is shown in Figure 6c. Figure 6a shows the image formed from selecting the lower section of the cluster.

Axis cluster (also linear clustering), as shown in Figure 8, normally means that there is little or no association between the two elements. The example shown in Figure 8 reveals at least two linear clusters along the length of the scatter diagrams axes linked to a spherical cluster at

the origin. This sample is from a weld flux material where the phases are isolated from each other and the individual elements exist in separate phases.

ii. Branches and Links between Clusters

Linking is the connection between two clusters, and is distinct from the correlation or anti-correlation of two elements (branching or oval clustering). Linking usually indicates the boundaries between phases within a material and, as such, can be an artefact due to the interaction volume of the beam within the specimen overlapping the two phases on its boundary [5]. There is also a possibility of the links containing small clusters or branches, as in the case of silicon on the boundary between aluminium and titanium shown in the silicon x-ray map, Figure 1c. If there is no link between two clusters, the phases are isolated from each other. This occurs when phases are within another phase, or where a high magnification is used that appears to change the association distribution. This can also be seen in Figure 8b, where the clusters are linked to the zero node and not to each other.

The interaction volume artefacts are very important and must be investigated to determine whether there is any possibility of reducing their affect. Lowering the excitation voltage is one way of improving this effect; another is preparing a thin section for transmission electron microscopy (TEM) mapping, which can reduce this effect to almost atomic dimensions.

Another feature normally observed with a cluster, is branching. Branching is defined as a link with a node at one end only, and is often referring to solid solutions (compositional variations) of the same phase or separate phases of similar solid solution. This is also similar

to linear clustering. Very small phases will also appear as branches and, furthermore, a solid solution can appear as a branch or smearing of the cluster, as shown in Figure 6b.

iii. Minor element distributions and the effect of the statistics of clusters and averaging.

The counting statistics from the x-ray map plays a crucial role on the quality of the scatter diagram obtained. Figure 6e shows a scatter diagram for cobalt and manganese from a high resolution x-ray map performed at low dwell time per point, as well as for trace and minor elements within the sample. As can be seen, the cluster has no clear indication of its concentration range. This observation usually occurs for either minor elemental distributions or from poor counting statistics or both, as in this case. Averaging the data creates an entirely different scenario. Once the data has been averaged to improve the statistics (Figure 6f), it becomes apparent that the cluster is still relatively spherical, but the manganese has shifted to the right indicating its presence in the sample. On analysis, the cluster was found to exist of two spherical distributions overlapping each other at 0.2% and 0.4wt%. Figure 6f appears oval shaped as the x-axis has a larger scale to accommodate other phases with higher concentrations in the sample. This often happens when averaging is introduced. What can start out looking like a spherical cluster often ends up with local variations. Thus, we can determine the manganese concentration very accurately by averaging many points in the image that are of the same phase. This averaging affect can also be seen in Figure 6b averaged from the raw data of Figure 6d.

6. Ternary and 3D Scatter Diagrams

The advantage of ternary and 3D scatter diagrams is that correlations between related phases can be visualised in a single diagram (Figure 9). This helps provide more detail that could easily be missed in 2D diagrams. However, they can also be misleading, because some details may still be hidden. The way to solve this problem is to use rotating 3D scatter diagrams that can provide information and reveal facts about a sample that might otherwise have been overlooked.

7. Conclusion

The use of scatter diagrams is a very powerful and useful technique for transforming x-ray maps from spatial to concentration dimensions and consequently allows more thorough examination of elemental and phase distributions in materials. The contributing pixels to each cluster observed in a scatter diagram can be used to reconstruct the spatial distribution of its associated chemical phase or boundary in a chemical image of the specimen.

One of the important aspects, when correlating elements, is to ensure that there is enough information in the data before beginning the process. This can be accomplished by simply observing the x-ray images for each of the elements in the sample. Those images that give the greatest contrast variation in real image information are usually the best ones for using as correlation elements. Data massaging techniques such as averaging also help in determining the final process.

A more accurate understanding of materials can be obtained through the use of not only two dimensional scatter diagrams but also through the use of two dimensional ternary scatter

diagrams and three dimensional scatter diagrams. One of the main functions of the scatter diagrams is to be able to use this function for all ‘like compositional areas’ of an image. When these have been extracted other properties of these areas can then be determined and analysed. Rotating three-dimensional and rotating two-dimensional diagrams help in our understanding of the complexity of the associated phases, but in the end we are interested in their spatial distribution and affect on the matrix. To this end it is important to be able to 1) plot individual areas from the image to the scatter diagram, 2) display areas on the image from the scatter diagram and 3) display all the pixels on the image for analysis. These selected analysis points may then be summed for a more accurate analysis in total or by selecting strategic areas on the image.

No matter what type of scatter diagram is used, many considerations are required to be taken into account for their correct interpretation. Indeed, for some samples it is not always necessary to even refer to the scatter diagrams. Simple colouring may be all that is needed, or even careful observation of the individual element distributions may also reveal the required information.

Acknowledgements

Contribution of samples and discussions with Darren Attard, Paul Huggett, Peter Lloyd and Matthew Phillips are greatly appreciated.

References

1. D. S. Bright and D. E. Newbury, “Concentration histogram imaging, Analytical Chemistry”, Vol. 63, No. 4 (1991) 243A.
2. N. Bonnet, “Preliminary investigation of two methods for the automatic handling of multivariate maps in microanalysis”, Ultramicroscopy, 57 (1995) 17-27.
3. P. G. Kenny, I. R. Barkshire and M. Prutton, “Three-dimensional scatter diagrams: application to surface analytical microscopy”, Ultramicroscopy, 56 (1994) 289-301.
4. P. Huggett, R. Wuhrer, B. Ben-Nissan and K. Moran, “A novel metallurgical bonding process and microstructural analysis of ferrous alloy composites”, Materials Forum, Vol. 29, Edited by J.F. Nie and M. Barnett, IMEA (2005) 83-88.
5. R. Wuhrer and K. Moran, “Artifacts in x-ray mapping”, AMAS VIII-The eight biennial symposium, University of Melbourne (2005) 109.

List of Figures

Figure 1: Titanium alloy bonded to an aluminium alloy by the vacuum casting method [4]. a) SE image of the interface between the two alloys and elemental x-ray maps of b) titanium, c) silicon and d) aluminium. Maps collected at 20keV, 512x512 pixel, 100msec/pixel and 7kcps. Width of field (WOF) = 288 microns.

Figure 2: Intensity histograms for each of the respective elements produced from the x-ray maps shown in Figure 1. a) titanium, b) aluminium and c) silicon.

Figure 3: Scatter diagram generated from the titanium distribution plotted against the aluminium distribution. The intensity distributions are from Figure 2.

Figure 4: The complete set of scatter diagrams showing 5 different clusters from the bond interface region in Figure 1. a) titanium versus silicon, b) titanium versus aluminium and c) silicon versus aluminium.

Figure 5: Slag material. a) Calcium x-ray map, b) magnesium x-ray map, c) titanium x-ray map, d) titanium-calcium scatter diagram and e) titanium-magnesium scatter diagram. Maps collected at 20kV (WOF=330um).Map collected at 256x256, 120msec/pixel and 2.5kcps.

Figure 6: Hard facing material bonded to a steel substrate. a) BSE image with low chrome region superimposed over image (the overlays are on the steel substrate and represent 24wt% Cr), b) scatter diagram for chromium and iron showing many of the different cluster types after averaging, c) BSE image with high chrome region superimposed over image and represents 28wt% Cr, d) chromium and iron original scatter diagram for Figure 6b prior to averaging, e) cobalt-manganese raw scatter diagram revealing a spherical cluster about zero point (the crosshairs represent 0% for each element) and the size is due to poor counting statistics, and f) scatter diagram that has had the data averaged to improve statistics, which allows small localized phases to be located. This appears to distort the manganese axis, which is actually due to different axis scale. The main cluster is now shifted to the right of the crosshairs. The manganese axis consists of at least two un-separated gaussian peaks centering on 0.2% and 0.4% manganese (quantitation determined from grouping multiple pixels on the

image). The main cluster is still approximately spherical, if the x-axis is set to the same axis scale. The square to the right of Figure 6f has been identified as a small localized phase enriched in manganese. Maps collected at 20keV, 512x512 pixel, 200msec/pixel and 7kcps (WOF=100um).

Figure 7: Example of zoning from a high chromium cast iron. a) Chromium x-ray map, b) iron x-ray map, c) quantitative scatter diagram created from iron-chromium x-ray maps and showing area of cluster selected and d) zoning image created by selecting a cluster of points and then superimposing these points on the SEM image. Maps collected at 20keV, 256x256 pixel, 4700msec/point and 2.5kcps (WOF = 155um).

Figure 8: Welding flux material. a) BSE image of particles and b) iron-calcium scatter diagram. Maps collected at 20keV, 512x512 pixel, 550msec/pixel and 2.5kcps (WOF=2.25mm). The scatter diagram reveals three main clusters existing.

Figure 9: a) Ternary scatter diagram and b) 3D scatter diagram which can be rotated for the results displayed in Figure 1.

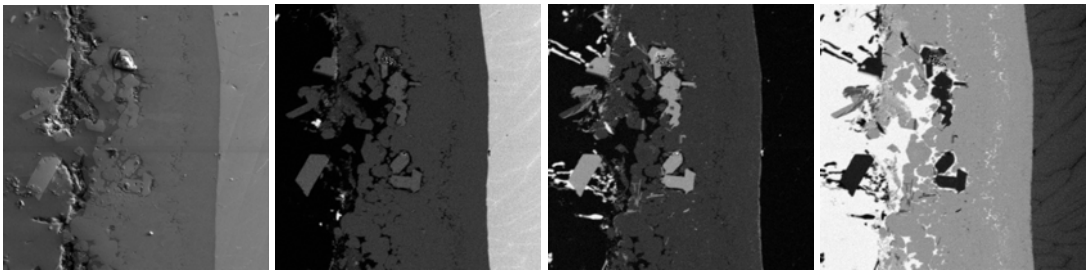

a. b. c. d.

Figure 1: Titanium alloy bonded to an aluminium alloy by the vacuum casting method [4]. a) SE image of the interface between the two alloys and elemental x-ray maps of b) titanium, c) silicon and d) aluminium. Maps collected at 20keV, 512x512 pixel, 100msec/pixel and 7kcps. Width of field (WOF) = 288 microns.

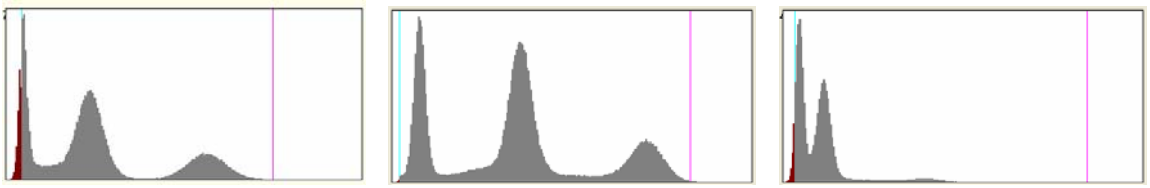

a. b. c.

Figure 2: Intensity histograms for each of the respective elements produced from the x-ray maps shown in Figure 1. a) titanium, b) aluminium and c) silicon.

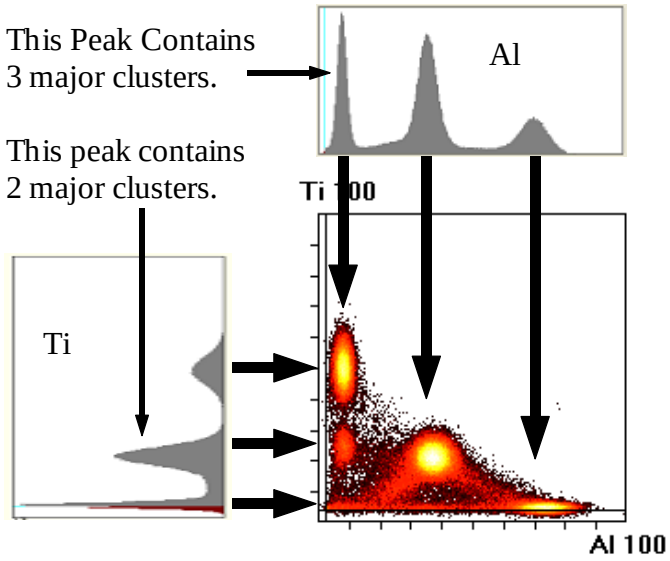

Figure 3: Scatter diagram generated from the titanium distribution plotted against the aluminium distribution. The intensity distributions are from Figure 2.

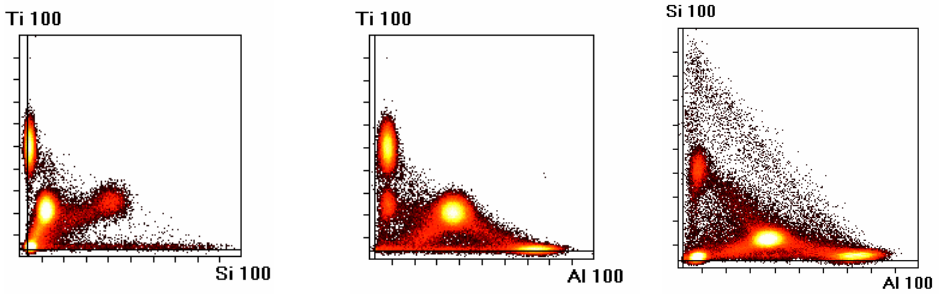

a. b. c.

Figure 4: The complete set of scatter diagrams showing 5 different clusters from the bond interface region in Figure 1. a) titanium versus silicon, b) titanium versus aluminium and c) silicon versus aluminium.

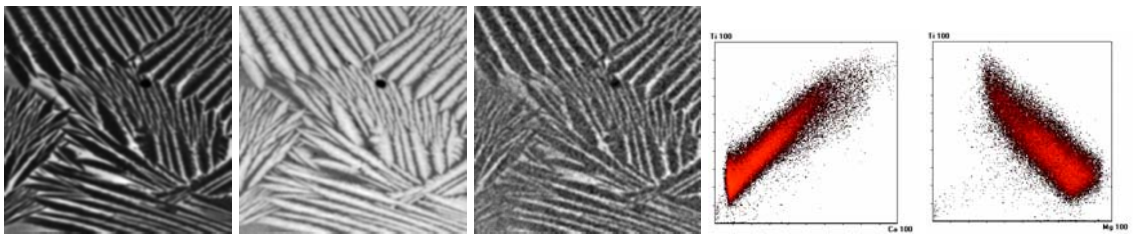

a. b. c. d. e.

Figure 5: Slag material. a) Calcium x-ray map, b) magnesium x-ray map, c) titanium x-ray map, d) titanium-calcium scatter diagram and e) titanium-magnesium scatter diagram. Maps collected at 20kV (WOF=330um).Map collected at 256x256, 120msec/pixel and 2.5kcps.

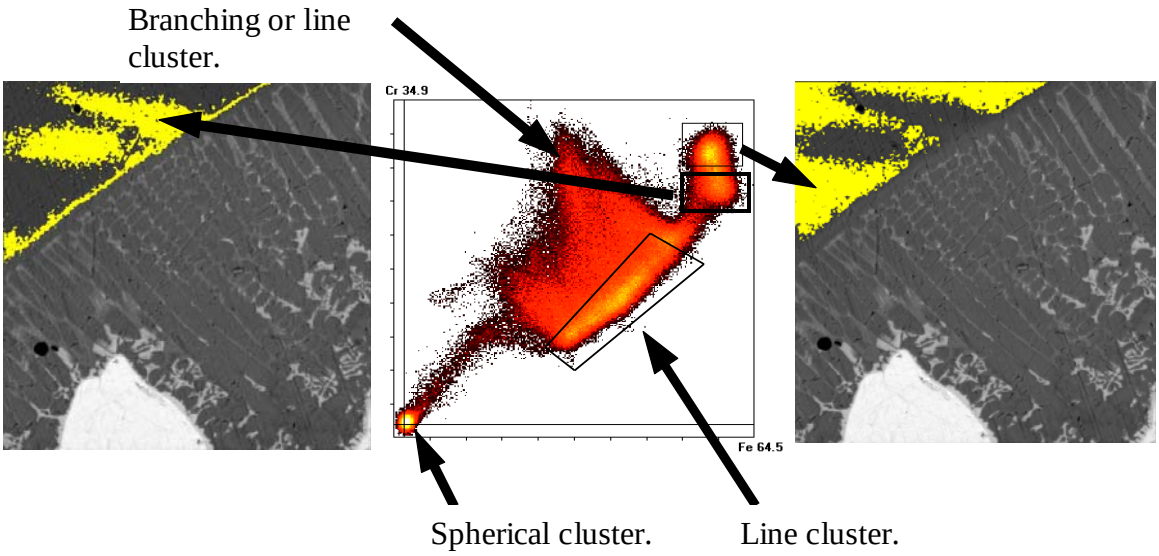

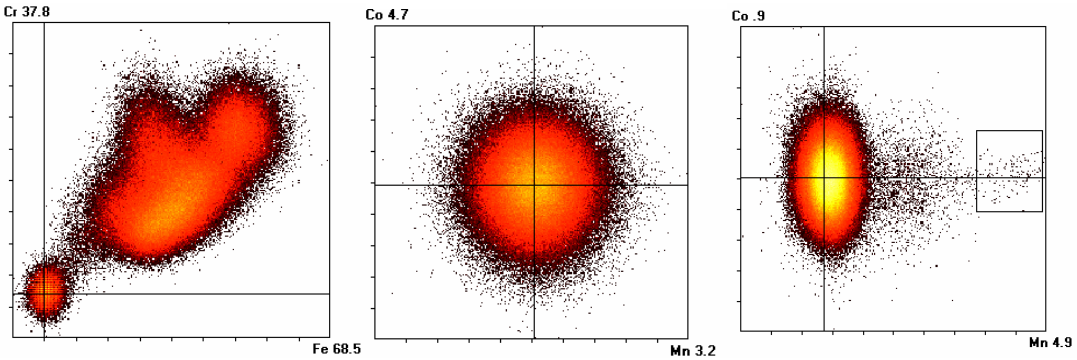

Figure 6: Hard facing material bonded to a steel substrate. a) BSE image with low chrome region superimposed over image (the overlays are on the steel substrate and represent 24wt% Cr), b) scatter diagram for chromium and iron showing many of the different cluster types after averaging, c) BSE image with high chrome region superimposed over image and represents 28wt% Cr, d) chromium and iron original scatter diagram for Figure 6b prior to

averaging, e) cobalt-manganese raw scatter diagram revealing a spherical cluster about zero point (the crosshairs represent 0% for each element) and the size is due to poor counting statistics, and f) scatter diagram that has had the data averaged to improve statistics, which allows small localized phases to be located. This appears to distort the manganese axis, which is actually due to different axis scale. The main cluster is now shifted to the right of the crosshairs. The manganese axis consists of at least two un-separated gaussian peaks centering on 0.1% and 0.3% manganese (quantitation determined from grouping multiple pixels on the image). The main cluster is still approximately spherical, if the x-axis is set to the same axis scale. The square to the right of Figure 6f has been identified as a small localized phase enriched in manganese. Maps collected at 20keV, 512x512 pixel, 200msec/pixel and 7kcps (WOF=100um).

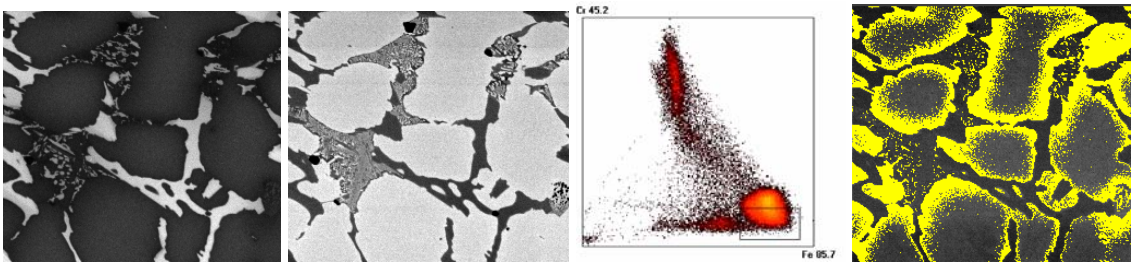

a b c d

Figure 7: Example of zoning from a high chromium cast iron. a) Chromium x-ray map, b) iron x-ray map, c) quantitative scatter diagram created from iron-chromium x-ray maps and showing area of cluster selected and d) zoning image created by selecting a cluster of points and then superimposing these points on the SEM image. Maps collected at 20keV, 256x256 pixel, 4700msec/point and 2.5kcps (WOF = 155um).

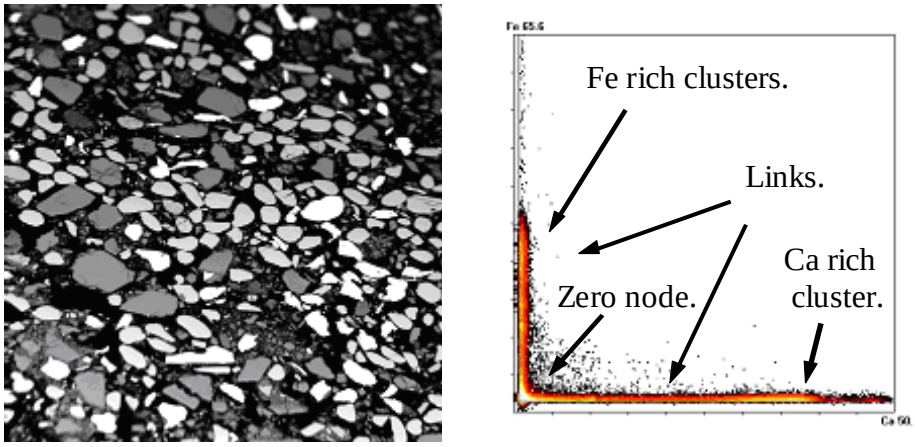

a. b.

Figure 8: Welding flux material. a) BSE image of particles and b) iron-calcium scatter diagram. Maps collected at 20keV, 512x512 pixel, 550msec/pixel and 2.5kcps (WOF=2.25mm). The scatter diagram reveals three main clusters existing.

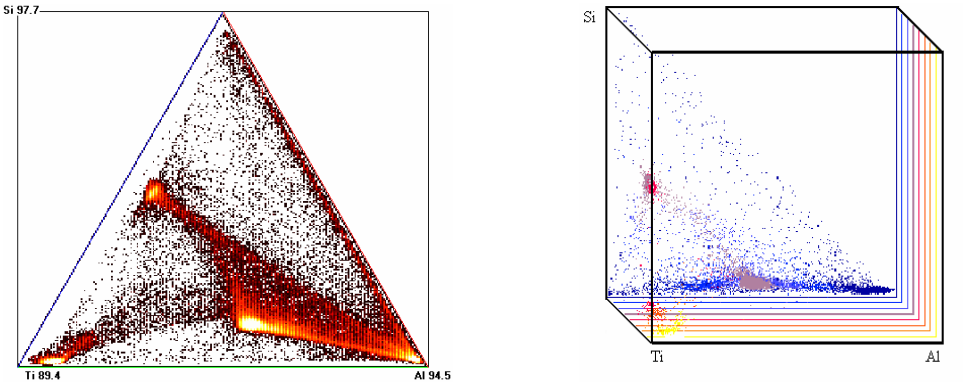

a. b.

Figure 9: a) Ternary scatter diagram and b) 3D scatter diagram which can be rotated for the results displayed in Figure 1.